Original Article

Evaluation of single-photon emission computed tomography images obtained with and without copper filter by segmentation

Subhash Chand Kheruka, Lalit Mohan Aggarwal[1], Neeraj Sharma[2], Umesh Chand Naithani[3], Anil Kumar Maurya[4], Sanjay Gambhir

Departments of Nuclear Medicine and [4]Radiotherapy, SGPGIMS, Lucknow, [1]Department of Radiotherapy and Radiation Medicine, Institute of Medical Sciences, Banaras Hindu University, [2]School of Biomedical Engineering, IIT, Banaras Hindu University, Varanasi, Uttar Pradesh, [3]Department of Physics, HNB University, Srinagar, Uttarakhand, India

ABSTRACT

Background: Measurement of accurate attenuation of photon flux in tissue is important to obtain reconstructed images using single-photon emission computed tomography (SPECT). Computed tomography (CT) scanner provides attenuation correction data for SPECT as well as anatomic information for diagnostic purposes. Segmentation is a process of dividing an image into regions having similar properties such as gray level, color, texture, brightness, and contrast. Image segmentation is an important tool for evaluation of medical images. X-ray beam used in CT scan is poly-energetic; therefore, we have used a copper filter to remove the low energy X-rays for obtaining correct attenuation factor. Images obtained with and without filters were quantitatively evaluated by segmentation method to avoid human error. **Materials and Methods:** Axial images of AAPM CT phantom were acquired with 3 mm copper filter (low intensity) and without copper filter (high intensity) using low-dose CT (140 kvp and 2.5 mA) of SPECT/CT system (Hawkeye, GE Healthcare). For segmentation Simulated Annealing Based Fuzzy c-means, algorithm is applied. Quantitative measurement of quality is done based on universal image quality index. Further, for the validation of attenuation correction map of filtered CT images, Jaszczak SPECT phantom was filled with 500 MBq of ^{99m}Tc and SPECT study was acquired. Low dose CT images were acquired for attenuation correction to be used for reconstruction of SPECT images. Another set of CT images were acquired after applying additional 3 mm copper filter. Two sets of axial SPECT images were reconstructed using attenuation map from both the CT images obtained without and with a filter. **Results and Conclusions:** When we applied Simulated Annealing Based Fuzzy c-means segmentation on both the CT images, the CT images with filter shows remarkable improvement and all the six section of the spheres in the Jaszczak SPECT phantom were clearly visualized.

Keywords: Copper filter, fuzzy c-means, Jaszczak single-photon emission computed tomography phantom, segmentation, single-photon emission computed tomography

INTRODUCTION

Measurement of accurate attenuation of photon flux in tissue is important to obtain reconstructed images using single-photon emission computed tomography (SPECT). Computed tomography (CT) scanner provides attenuation correction data for SPECT as well as anatomic information for diagnostic purposes. X-ray beam used in CT scan is poly-energetic, therefore, we have used a copper filter to remove the low energy X-rays to obtain more accurate attenuation factor as described by Kheruka *et al.*[1] Images

Address for correspondence:
Dr. Lalit Mohan Aggarwal, Department of Radiotherapy and Radiation Medicine, Institute of Medical Sciences, Banaras Hindu University, Varanasi - 221 005, Uttar Pradesh, India.
E-mail: lmaggarwal@yahoo.com

Access this article online

Quick Response Code:

Website: www.ijnm.in

DOI: 10.4103/0972-3919.178260

How to cite this article: Kheruka SC, Aggarwal LM, Sharma N, Naithani UC, Maurya AK, Gambhir S. Evaluation of single-photon emission computed tomography images obtained with and without copper filter by segmentation. Indian J Nucl Med 2016;31:114-8.

obtained with and without filters were quantitatively evaluated by segmentation method to avoid human error.

Segmentation is a process of dividing an image into regions having similar properties such as gray level, color, texture, brightness, and contrast. Image segmentation is an important tool for evaluation of medical images.[2-6] In nuclear medicine, segmentation of images could play an important role to know the size and exact extent of the lesion. The techniques available for segmentation of images can be broadly classified into two categories.

- Techniques based on Gray levels, this can be further sub-classified as (a) amplitude segmentation methods based on histogram features,[7] (b) edge based segmentation and (c) region based segmentation[8]
- Techniques based on textural features.[9]

Image segmentation based on textural features

In medical image processing, segmentation based on gray level does not give the desired results whereas segmentation based on textural feature methods gives more reliable results.[10,11] Therefore, textural features are extensively used in the analysis of medical images.[12-14] Various methods available for textural feature extraction and classification based on the above approaches are: (a) Co-occurrence matrix method based on statistical description of gray level of an image,[15,16] (b) gray level run length method[17] (c) fractal texture description method,[18] (d) syntactic method,[19] and (e) Fourier filter method.[20] Further, as a comparison between the above-mentioned textures based approaches, spectral frequency-based methods are less efficient while statistical methods are particularly useful for random patterns/textures. Whereas for complex patterns, syntactic or structural methods give better results. Therefore, in this study the textural properties have been computed using first-order statistics or second-order statistics that are computed from spatial gray-level co-occurrence matrices (GLCMs) for evaluation of images.

MATERIALS AND METHODS

In this study, we have used AAPM CT phantom and Jaszczak SPECT phantom to obtain CT and SPECT images. Axial images of CT phantom were acquired with 3 mm copper filter (low intensity) and without copper filter (high intensity). All the images were acquired with Hawkeye, GE Healthcare SPECT/CT system using low-dose CT at 140 kvp, 2.5 mA and 400 mm field of view as shown in Figure 1a and b. To generate correct air correction table in the presence or absence of filters, the daily X-ray calibration procedure has been repeated with and without 3.0 mm copper filter. In this process, the system takes full rotation without any object between the X-ray source and detector (i.e., in air) and another full rotation with daily quality control phantom placed in between X-ray source and detector.

For the validation of attenuation correction map of filtered CT images, Jaszczak SPECT phantom was filled with 500 MBq of

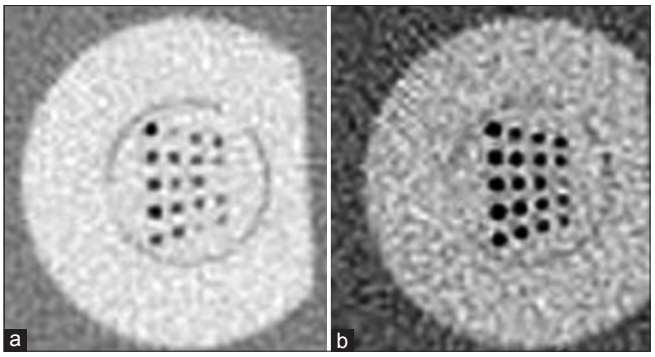

Figure 1: Computed tomography phantom cross-sectional images of resolution pattern. (a) Without copper filter, (b) with copper filter

^{99m}Tc and SPECT study was acquired in 64 × 64 matrix size for all 60 views over 360° rotation. Low dose CT images were acquired for attenuation correction to be used for reconstruction of SPECT images. Another set of CT images were acquired after applying additional 3 mm copper filter. Two sets of axial SPECT images were reconstructed using attenuation map from both the CT images obtained without and with filter [Figure 2]. Ordered subsets expectation maximization was used for reconstruction of SPECT images.

Jaszczak SPECT phantom consisted of 6 solid spheres having diameter 9.5 mm, 12.7 mm, 15.9 mm, 19.1 mm, 25.4 mm, and 31.8 mm. To see the effect of filtration on the CT and SPECT images, the cross-sections of only large 3 solid spheres were analyzed quantitatively by segmentation method.

Segmentation method as described by Sharma *et al.*[21] was applied on the CT images (without and with filter) and SPECT Images of Jaszczak SPECT phantom obtained using without and with filter CT attenuation maps [Figure 3]. The textural features of obtained image were calculated. The textural properties have been derived using the first-order statistics and second-order statistics that were computed from spatial GLCMs. For segmentation Simulated Annealing Based Fuzzy c-means algorithm was applied.

Further, the segmented images were analyzed quantitatively by measuring the diameters of the spheres in all set of the images, and the cross section areas of the spheres were calculated. Quantitative measurement of quality is done based on a universal image quality index (UIQI) as proposed by Wang and Bovik.[22]

Validation of filtered computed tomography attenuation correction map

Quantitative analysis of image quality

For quantitative analysis of image quality, we have used CT phantom, and images were acquired with 3 mm copper filter (low intensity) and without copper filter (high intensity) using low-dose CT (140 kvp and 2.5 mA). We have used Q, the UIQI as proposed by Wang and Bovik[22] to measure the image quality, this index measures image distortion as

a combination of three factors: (i) Loss of correlation, (ii) luminance distortion, and (iii) contrast distortion. The value of Q is computed as follows:

$$Q = \frac{4\sigma_{xy}\,\mu_x\mu_y}{\left[\sigma_x^2+\sigma_y^2\right]\left[\mu_x^2+\mu_y^2\right]}$$

Where μ_x and μ_y are mean values, σ_x and σ_y are standard deviations of original image $X = \{x_i \mid i = 1, 2, N\}$ and image acquired $Y = \{y_i \mid i = 1, 2, \ldots N\}$ whose quality is to be measured, respectively and are computed as follows:

$$\mu_x = \frac{1}{N}\sum_{i=1}^{N} x_i$$

$$\mu_y = \frac{1}{N}\sum_{i=1}^{N} y_i$$

$$\sigma_x = \sqrt{\frac{1}{N-1}\sum_{i=1}^{N}(x_i-\mu_x)^2}$$

$$\sigma_y = \sqrt{\frac{1}{N-1}\sum_{i=1}^{N}(y_i-\mu_y)^2}$$

$$\sigma_{xy} = \frac{1}{N-1}\sum_{i=1}^{N}(x_i-\mu_x)(y_i-\mu_y)$$

The dynamic range of Q is (−1.0 to 1.0), 1.0 is the best value which is achieved if $y_i = x_i$ i.e., the image quality of acquired image is same as that of the original image (phantom image) and −1.0 means a poor image quality and correlation.

Further, Mean Square Error (MSE) is also widely used as mathematical measure for measuring the image quality of images[23] and is measured as follows:

$$MSE = \frac{1}{N}\sum_{i=1}^{N}[x_i - y_i]^1$$

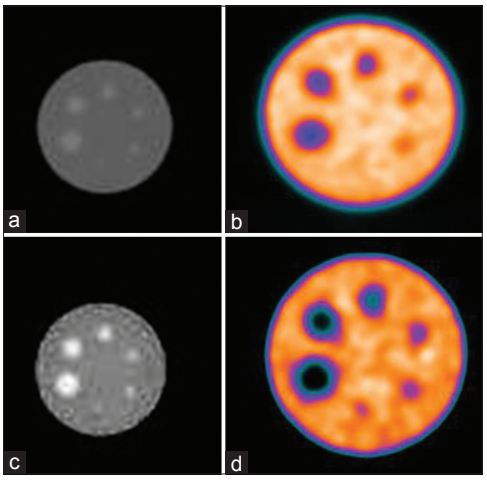

Figure 2: Axial computed tomography and single-photon emission computed tomography images of Jaszczak single-photon emission computed tomography phantom acquired without and with a copper filter. (a) Axial computed tomography image acquired without any additional filter, (b) reconstructed single-photon emission computed tomography image using the attenuation map from (a), (c) axial computed tomography image acquired with additional 3 mm copper filter, (d) reconstructed single-photon emission computed tomography image using the attenuation map from (c)

RESULTS

Images obtained with 3 mm copper filters were having better resolution than the images obtained without a copper filter as shown in Figure 1. UIQI Q was used to measure the quality of image acquired for CT phantom under different conditions, i.e. at the different hardness of X-ray beam and the results of same along with the value of Q and MSE as shown in Table 1. Quality index of the images obtained with the filter was higher, and MSE was low as compared to images obtained without a filter.

Analysis of the results

The segmented CT and SPECT images of Jaszczak SPECT phantom showed good consistency in terms of a number of pixels and area of the circular cross-section of the spheres in filtered images whereas no correlation has been found in the segmented images without a filter. When we applied Simulated Annealing Based Fuzzy c-means segmentation on both the CT images with and without a copper filter, the CT images with filter showed remarkable improvement and all the six section of the spheres were clearly visualized. When we applied same segmentation method on the reconstructed SPECT images obtained without and with filter CT attenuation maps, the same observations were noted [Figure 3]. Segmented

Table 1: Quality index and MSE at different hardness of the X-ray beam using CT phantom

Cross section of original phantom image	Image acquired	
	Without copper filter	With copper filter
Q=1.0	Q=0.7722	Q=0.9655
MSE=0.0	MSE=18.5364	MSE=6.0485

CT: Computed tomography, MSE: Mean square error

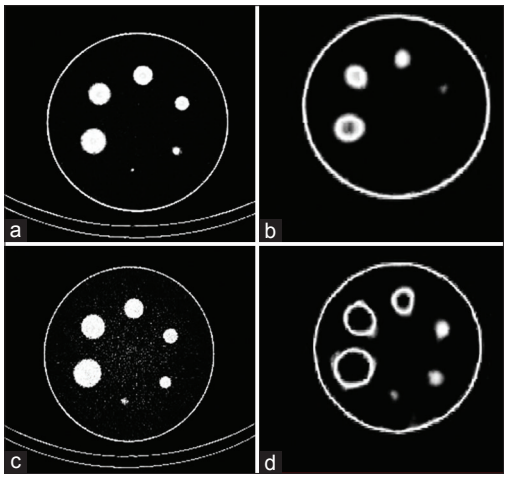

Figure 3: Segmented computed tomography and single-photon emission computed tomography images of Jaszczak single-photon emission computed tomography phantom. (a) Segmented computed tomography image without filter, (b) segmented single-photon emission computed tomography image without filter, (c) segmented computed tomography image with filter, (d) segmented single-photon emission computed tomography image with filter

Table 2: Measurement of diameter of bigger three spheres

Original diameter	Without copper filter				With 3.0 mm copper filter			
	CT	Error (%)	SPECT	Error (%)	CT	Error (%)	SPECT	Error (%)
31.8	26.4	17.0	10.9	65.7	29.4	7.5	29.0	8.8
25.4	22.1	13.0	9.6	62.2	24.8	2.4	24.7	2.8
19.1	18.6	2.6	3.6	81.2	20.1	−5.2	14.0	26.7

CT: Computed tomography, SPECT: Single-photon emission computed tomography

SPECT phantom image reconstructed using without filter CT attenuation map showed only four circular cross-sections of the bigger spheres. Whereas, with filter showed all the six cross-sections of the spheres very clearly. We have measured the diameter of the bigger three spheres for comparison and details are given in Table 2. As expected the mean intensity observed in the circular cross-sections of the spheres in the SPECT images reconstructed with filtered CT images were found quite low as no activity was contained inside the spheres. Cold area (low activity) was very well visualized for three bigger spheres in SPECT images with filter whereas it could be seen only for one sphere in unfiltered image.

The original diameters of the largest three spheres were 31.8 mm, 25.4 mm, and 19.1 mm. The computed diameters on without filter CT and SPECT images are given in Table 2, which shows large variations of 17%, 13%, 2.6%, and 65.7%, 62.2%, 81.2 for CT and SPECT images respectively. On applying additional 3 mm copper filter, the measured diameter of the targets on CT and SPECT images became 29.4 mm, 24.8 mm, 20.1 mm, and 28.0 mm, 24.7 mm, 14.0 mm, respectively showing the variation of 7.5%, 2.4%, -5.2%, and 8.8%, 2.8%, 26.7% from the calculated values. This study shows that the estimations became more accurate on CT and SPECT images after applying additional 3 mm copper filter. Moreover, the measurement of diameters of three big spheres on filter CT and SPECT images are in good agreement in contrast to large variations observed in that of without filtered images.

DISCUSSION

Scatter-induced artifacts in the CT image can have a similar appearance in the emission images and can severely distort the attenuation-corrected images, making these images effectively useless as reported by Nuyts *et al.* on positron emission tomography (PET)/CT images.[24] Attenuation correction problem in SPECT and PET imaging has been studied by several authors, and various methods have been proposed to tackle this problem.[25-27] The only option offered by all manufacturers of SPECT scanners is to incorporate X-ray CT-based attenuation correction algorithms in their systems, and it is bilinear and hybrid scaling methods. This method works well for clinical procedures when X-ray beam is monoenergetic. However, X-ray beam used in SPECT with low-dose CT is poly-energetic. There are other remaining challenges that can cause errors in the converted attenuation correction factors caused by contrast agents and respiratory motion as well as truncation and beam hardening. Errors that are present in the CT-based attenuation image have the potential of introducing bias or artifacts in the attenuation corrected SPECT emission image as studied by Kinahan *et al.* for PET/CT systems.[28] Uncorrected beam hardening and scatter build-up reduces measured attenuation along the lines of high attenuation. Therefore, there is need to remove these low energy X-ray component, which we have achieved by using a copper filter. Therefore, images obtained with 3.0 mm copper filter for attenuation correction are superior as it removes the low energies X-ray beam from the primary beam. The results obtained with segmentation were in agreement with the results obtained by Kheruka *et al.*[1] Further, segmentation of the images was useful in the analysis of the images.

CONCLUSION

On the basis of this preliminary study and use of copper filter by Kheruka *et al.*,[1] we could conclude that use of 3 mm copper filter to harden the X-ray beam is optimal for removing the artifacts without causing any significant reduction in the photon flux of the resulting X-ray beam. We found that image quality has improved with almost no artifact; a very common problem seen in inadequately filtered X-ray beams. It could be established that the images acquired with the filter are of good quality as compared to images acquired without 3.00 mm copper filter and are free from bloom artifact. This study also showed that segmentation of images is an important tool in analyzing the images which avoid the human error.

Financial support and sponsorship

Nil.

Conflicts of interest

There are no conflicts of interest.

REFERENCES

1. Kheruka S, Naithani U, Maurya A, Painuly N, Aggarwal L, Gambhir S. A study to improve the image quality in low-dose computed tomography (SPECT) using filtration. Indian J Nucl Med 2011;26:14-21.
2. Sharma N, Aggarwal LM. Automated medical image segmentation techniques. J Med Phys 2010;35:3-14.
3. Petitjean C, Dacher JN. A review of segmentation methods in short axis cardiac MR images. Med Image Anal 2011;15:169-84.
4. Maity S, Sil J. Feature Extraction of Bone Scintigraphy for Diagnosis of Diseases. International Conference on Communication Systems and Network Technologies (CSNT); 2012. p. 179-83.
5. Qranfal J, Hochbaum D, Tanoh G. Experimental Analysis of the MRF Algorithm for Segmentation of Noisy Medical Images. Algorithmic Operations Research, North America; 2012.

6. Umamaheswari J, Radhamani G. An amalgam approach for DICOM image classification and recognition. World Acad Sci Eng Technol 2012;62:807-12.
7. Ramesh N, Yoo JH, Sethi IK. Thresholding based on histogram approximation. IEEE Proc Vis Image Signal Process 1995;142:271-9.
8. Sharma N, Ray AK. Computer Aided Segmentation of Medical Images Based on Hybridized Approach of Edge and Region Based Techniques. Proceedings of International Conference on Mathematical Biology', Mathematical Biology Recent Trends by Anamaya Publishers; 2006. p. 150-5.
9. Sharma N, Ray AK, Sharma S, Shukla KK, Pradhan S, Aggarwal LM. Segmentation and classification of medical images using texture-primitive features: Application of BAM-type artificial neural network. J Med Phys 2008;33:119-26.
10. Wang Z, Gierriero A, Sario M. Comparison of several approaches for segmentation of texture images. Pattern Recognit Lett 1996;17:509-21.
11. Tesar L, Shimizu A, Smutek D, Kobatake H, Nawano S. Medical image analysis of 3D CT images based on extension of Haralick texture features. Comput Med Imaging Graph 2008;32:513-20.
12. Xie J, Jiang Y, Tsui HT. Segmentation of kidney from ultrasound images based on texture and shape priors. IEEE Trans Med Imaging 2005;24:45-57.
13. Wu CM, Chen YC, Hsieh KS. Texture features for classification of ultrasonic liver images. IEEE Trans Med Imaging 1992;11:141-52.
14. Miller P, Astley S. Classification of breast tissue by texture analysis. Image Vis Comput 1992;10:277-82.
15. Argenti F, Alparone L, Benelli G. Fast algorithm for texture analysis using co-occurance matrices. Radar and Signal Processing, IEE Proceedings F1990;137:443-8.
16. Haralick RM, Shanmugan K, Dinstein I. Textural features for image classification. IEEE Trans Syst Man Cybern 1973;3:610-22.
17. Chu A, Sehgal CM, Greenleaf JF. Use of gray value distribution of run lengths for texture analysis. Pattern Recogni Lett 1990;6:415-9.
18. Chaudhuri BB, Sarkar N. Texture segmentation using fractal dimension. IEEE Trans Pattern Anal Mach Intell 1995;17:72-7.
19. Lu SY, Fu KS. A syntactic approach to texture analysis. Comput Graph Image Process 1978;7:303-30.
20. Azencott R, Wang J, Younes L. Texture classification using windowed fourier filters. IEEE Trans Pattern Anal Mach Intell 1997;19:148-53.
21. Sharma N, Ray AK, Sharma S, Shukla KK, Pradhan S, Aggarwal LM. Segmentation of medical images using simulated annealing based fuzzy C means algorithm. Int J Biomed Eng Technol 2009;2:260-78.
22. Wang Z, Bovik AC. A universal image quality index. IEEE Signal Process Lett 2002;9:81-4.
23. Avcıbas I, Sankur B, Sayood K. Statistical evaluation of image quality measures. J Electron Imaging 2002;11:206-23.
24. Nuyts J, Bequé D, Dupont P, Mortelmans L. A concave prior penalizing relative differences for maximum-a-posteriori reconstruction in emission tomography. IEEE Trans Nucl Sci 2002;49:56-60.
25. Hamann M, Aldridge M, Dickson J, Endozo R, Lozhkin K, Hutton BF. Evaluation of a low-dose/slow-rotating SPECT-CT system. Phys Med Biol 2008;53:2495-508.
26. LaCroix KJ, Tsui BM, Hasegawa BH, Brown JK. Investigation of the use of X-ray CT images for attenuation compensation in SPECT. IEEE Trans Nucl Sci 1994;41:2793-9.
27. Fricke E, Fricke H, Weise R, Kammeier A, Hagedorn R, Lotz N, *et al*. Attenuation correction of myocardial SPECT perfusion images with low-dose CT: Evaluation of the method by comparison with perfusion PET. J Nucl Med 2005;46:736-44.
28. Kinahan PE, Hasegawa BH, Beyer T. X-ray-based attenuation correction for positron emission tomography/computed tomography scanners. Semin Nucl Med 2003;33:166-79.